Available online at www.sciencedirect.com
SCIENCE DIRECT®
Biosensors and Bioelectronics 19 (2004) 1371–1376
BIOSENSORS & BIOELECTRONICS
www.elsevier.com/locate/bios

High-speed label-free detection by spinning-disk micro-interferometry

Manoj M. Varma [a], Halina D. Inerowicz [b], Fred E. Regnier [b], David D. Nolte [a,*]

[a] *Adaptive Optics and Biophotonics Laboratory, Department of Physics, Purdue University, West Lafayette, IN 47907-2036, USA*
[b] *Department of Chemistry, Purdue University, West Lafayette, IN 47907,USA*

Abstract

Spinning-disk interferometers are a new class of analytic sensors to detect immobilized biomolecules with high speed and high sensitivity. The disks are composed of a large number of surface-normal self-referencing interferometers, analogous to an optical CD, but operating on the principle of microdiffraction quadrature that achieves sensitive linear detection of bound molecules. The surface-normal structures have a small footprint of only 20 μm each, allowing potential integration to over a million interferometric elements per disk. We have fabricated interferometric microstructures on silicon and on dielectric mirror disks to demonstrate the basic principles of the BioCD. We have detected the presence of immobilized anti-mouse IgG and the specific binding of 10 femtomol of mouse IgG at a sampling rate of 100 kilo-samples/s, while also demonstrating negligible non-specific binding. This technique provides a label-free method that could potentially screen hundreds to thousands of proteins per disk.

Keywords: Multi-analyte assays; Interferometry; Bio-sensors; Proteomics; Surface-normal; Direct detection; Shot-noise limit; High-density; Self-referencing; Spinning disk; Attomoles

1. Introduction

The need for high-thoughput multi-analyte biosensors in the emerging areas of genomics and proteomics cannot be overemphasized. Issues involved in the design of such biosensors include the high multiplicity of the biological binding sites that are needed for a complete assay which can number many thousands depending on the application. Even when biological receptors are exposed to the target molecules only a few may bind, and it is important to identify these in as short a time as possible. In such applications, it is also important to screen for many different target molecules at the same time. The techniques to perform such multi-analyte immunoassays have been drawn extensively from the technology of gene chips. Gene chips rely on the ability to print micro-arrays with many receptors on a single chip (MacBeath and Schreiber, 2000). Imaging detection of multi-analyte micro-array immunoassays is performed routinely (Silzel et al., 1998). Such approaches rely on the optical properties of the immunoassay, mainly relying on fluorescence (Ostroff et al., 1998). The throughput of such sensors is limited by the speed of the optical read-out even in the case of micro-spot assays. Fluorescence of the tagged molecules is detected using confocal microscopes and sensitive photo-detectors, but the low intensity of fluorescent radiation requires long integration times.

Several sensors have been developed on the basis of interferometry, as in the case of waveguides and grating couplers (Gao et al., 1995; Kunz, 1997; Jenison et al., 2001; Hanel and Gauglitz, 2002; Brecht et al., 1993; Fattinger et al., 1993). These approaches use static structures which prevent repetitive scanning and thus lack the high-speed capabilities of the technique that we describe here. We use the well-established technology of the optical CD to develop ultra high-throughput immunological assays performed on a single spinning disc with sampling rates as high as a mega sample/s sampling potentially a million separate micro-diffraction elements on a single BioCD. This would represent an improvement, by many orders of magnitude, in the throughput of immunological assays.

Commercially available compact discs (CDs) consist of concentrically-arranged tracks of pits that are half a micron wide and separated by 1.6 μm (Pohlmann, 1992). The information on a CD is read out by focusing a laser spot onto these pits and observing the far-field diffraction. The depth of the pits is a quarter of the wavelength of the laser

* Corresponding author. Tel.: +1-765-494-3013; fax: +1-765-494-0706.
E-mail address: nolte@physics.purdue.edu (D.D. Nolte).

0956-5663/$ – see front matter © 2004 Elsevier B.V. All rights reserved.
doi:10.1016/j.bios.2003.12.033

used for read-out. This depth difference between the pit and the land results in a phase difference of π between the light reflected off the pit and the light reflected off the land and leads to destructive interference at the detector, placed along the optic axis in the far-field. Thus each pit acts as a micro-interferometer, and an optical CD is a device with a billion such micro-interferometers. Biomolecules placed directly on a commercial CD have been detected using bit error rates during digital readout (La Clair and Burkart, 2003), but this approach is not intrinsically interferometric. We previously demonstrated the importance of operating in interferometric quadrature to achieve high sensitivity (Varma et al., 2003).

In this paper, we describe the fabrication of microstructures on silicon and dielectric mirror disks that act as microscopic interferometers, as on an optical CD, but operating in quadrature with maximum linear sensitivity, unlike a digital CD. These interferometers are printed with antibodies and binding of specific antigens is detected in the far-field diffraction as an amplitude change that is sampled at high speed as the disk rotates.

2. Fabrication and experimental setup

The BioCD is fabricated by evaporating gold ridges on a 3 in. silicon wafer or on a 2 in. dielectric mirror disk in a radial pattern as shown in Fig. 1. There are 1024 gold lines arranged in a radial pattern of spokes. These gold spokes are 20 μm wide and are deposited to a thickness of $\lambda/8 = 79.1$ nm, putting them in the quadrature condition for read-out with a 632.8 nm He–Ne laser.

The primary advantage of this ridge-based design over a design based on pits is that the gold ridges provide a simple means to immobilize macromolecules such as antibodies on the interferometric structures. By using alkanethiols as a bridge between the gold and the macromolecule, we immobilize antibodies on the gold spokes alone, thus making a selective pattern of antibodies on the wafer. By using polydimethylsiloxane (PDMS) stamps we immobilize antibodies on the gold pattern only in selected annuli of interest (Bernard et al., 2000). These annuli can also be created by incubating annular regions of the thiolated substrate with antibodies in solution. Thus a single wafer can have regions with and without antibodies, providing a means of control as we test for antigen binding events in the regions with antibody.

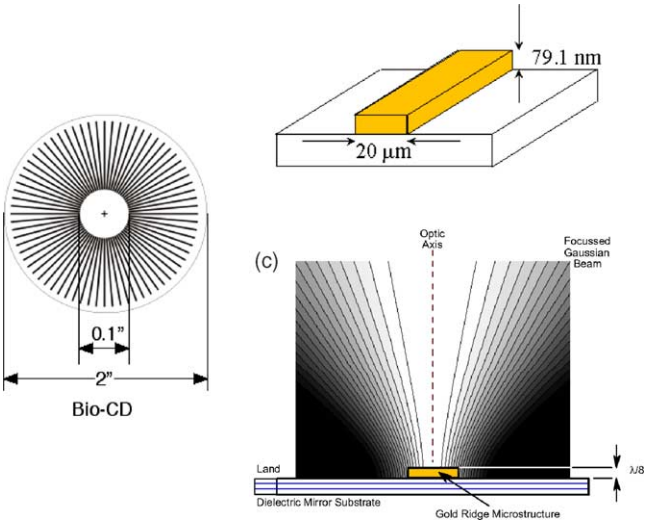

Fig. 1. Schematic of the arrangement of the gold lines on the BioCD. There are 1024 gold elements on a 2 in. disk. The spokes are illuminated by a focussed Gaussian beam in a configuration where 50% of the intensity falls on the land and 50% falls on the gold microstructure.

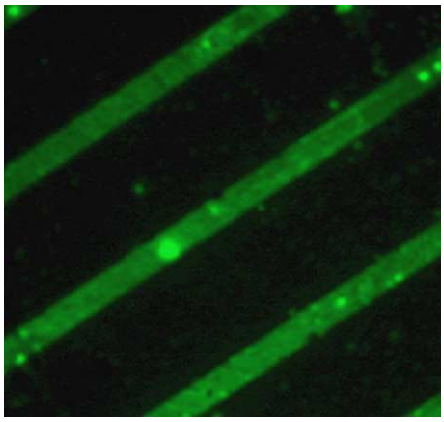

Fig. 2. Fluorescence image of immobilized BSA on the gold spokes of the BioCD. The immobilization is achieved through a thiol bridge that is highly selective to the gold spokes.

To validate the selective immobilization on the gold microstructures, Fig. 2 shows a fluorescence image from bovine serum albumin (BSA) immobilized on a BioCD. The BSA molecules were tagged with fluorescein. In the procedure for immobilization, the BioCD was treated with a 10 mM solution of hexa-decane-thiol in ethanol for 12–15 hours that deposited a thiol layer on the gold spokes. The thiolated disk was then treated with fluorescein-conjugated bovine serum albumin (200 μg/ml), immobilizing BSA selectively on the gold spokes. As the fluorescence image shows, the pattern of BSA is well defined and demonstrates the effectiveness of the gold-ridge approach in immobilizing antibodies.

Interferometers have a universal response curve, shown in Fig. 3a, with a half-intensity point defined by quadrature, when the signal and the reference waves are out of phase by ninety degrees and when the intensity versus phase has the highest slope. The calculated far-field diffraction patterns for three ridge heights $h = 0$, $\lambda/8$ and $\lambda/4$ (corresponding to land, quadrature, and conventional digital CD) are shown in Fig. 3b. Maximum linear sensitivity to small optical perturbations is achieved by operating the interferometer near quadrature. Shot noise-limited detection of optical path length changes down to a billionth-lambda is achievable under these conditions.

When a macromolecule is immobilized on a spoke, it introduces an additional phase (neglecting near-field effects)

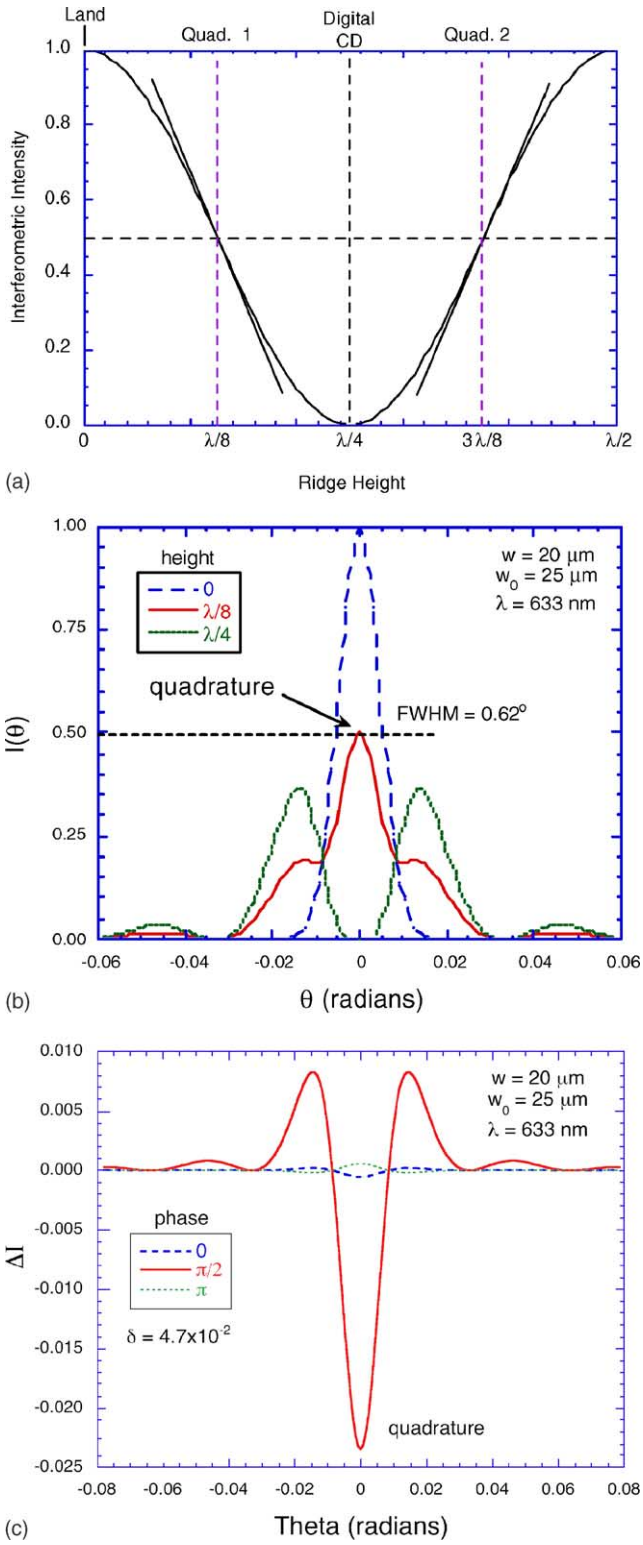

Fig. 3. (a) Universal response curve of a two-port interferometer shown here as a function of the height of the microstructure. A conventional digital CD alternates between the land and the point of destructive interference at λ/4. For the BioCD, quadrature is achieved at ridge heights of λ/8 and 3λ/8, where the maximum slope occurs. (b) Far-field diffraction patterns are shown for the cases of $h = 0$, λ/8 and λ/4. (c) Differential intensity response to a monolayer of immobilized biomolecules with mean height of 8 nm.

of

$$\delta\phi = \frac{4\pi}{\lambda}(n-1)d \tag{1}$$

where n is the effective refractive index of the biolayer and d is the biolayer thickness. This additional phase modifies the power detected at quadrature according to

$$\delta P = P_0 \frac{2\pi}{\lambda}(n-1)d \tag{2}$$

where P_0 is the power detected when the beam is incident on the land alone. The calculated response of the far-field diffraction to the additional phase load of a single monolayer of immobilized molecules is shown in Fig. 3c for ridge heights of $h = 0$, λ/8 and λ/4. The quadrature condition clearly leads to the strongest change in the signal. The signal is also linear in d, while for CDs the signal is quadratic in d.

3. Results and discussion

A schematic of the experimental layout is shown in Fig. 4. The laser beam is focused by a 10× objective lens onto the gold microstrips on the BioCD placed on a photoresist spinner. An image plane of the spoke structure is formed at a distance of 0.6 m from the disk with a magnification of $M = 200$. A 10 cm focal length lens is then used to perform a Fourier transform of the image of the gold microstrip to obtain the far-field signal at the Fourier plane. A photodetector placed at the Fourier plane monitors the far-field signals. A 25 μm pinhole is used to selectively pass the diffraction peak on the optic axis while blocking the higher-angle diffraction. The signal from the photodetector is sent to a preamplifier and then to a digital oscilloscope where direct time traces of the probe laser from the disk are monitored and captured for analysis. To achieve high sampling rates, the BioCD is mounted on a spinning platform capable of achieving speeds on the order of 6000 rpm, and detection is done while the device is spinning. We use a conventional photo-resist spinner (model P6204, SCS) as the rotating platform.

The 632.8 nm collimated He–Ne laser beam is focused to a waist diameter of between 40 and 80 μm at the disk surface. As the BioCD rotates at 6000 rpm, quadrature is achieved when the beam symmetrically straddles the gold

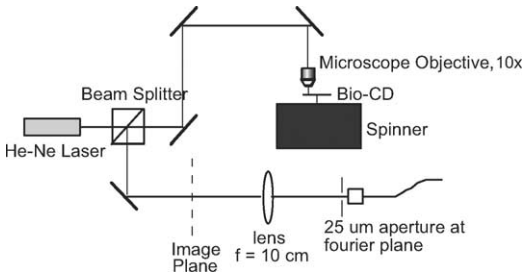

Fig. 4. Schematic of the experimental setup to detect the far-field diffraction from the BioCD.

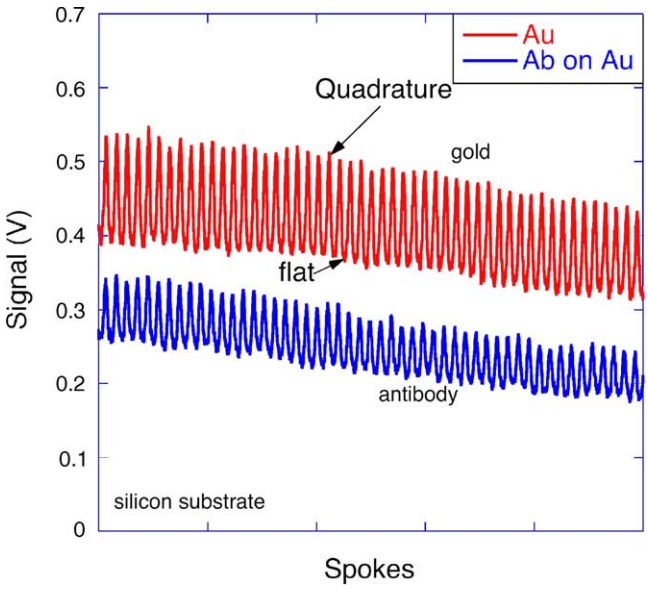

Fig. 5. Modulation of the far-field signal in the presence of an immobilized macro-molecule film. The data are offset to show the traces more clearly.

spoke. At other times the beam merely reflects off the land. At quadrature, the far-field diffraction intensity drops by approximately 50% compared to the intensity from the bare substrate (in the case of a laser mirror substrate). This results in the formation of peaks and dips in the oscilloscope trace, with the dips representing the interferometric signal in quadrature.

Fig. 5 shows the raw signal captured as a function of time by the oscilloscope in the presence of BSA immobilized on the gold spokes on a silicon wafer compared to a wafer with only gold (the offset between the curves is simply for ease of viewing). There is a clear decrease in the peak–peak difference of the signal caused by the immobilization of BSA on the gold spokes. When a silicon wafer is used as the substrate, the land has a 34% reflectance compared to the 100% reflectance of the gold microstructure. This situation flips the order of land and quadrature reflectance, with the land occurring as the dips and quadrature as the peaks in the oscilloscope time trace. When the BSA binds to the gold, it decreases the intensity of the peaks, and thus causes a decrease in the peak–peak signal values, as observed in the figure.

3.1. Specific binding

To test the ability of the BioCD to detect the presence of antigens in an sample, we immobilized anti-mouse IgG on an annular region roughly covering half the area of a silicon substrate with $h = \lambda/8$ gold spokes. We incubated a second annular region, contained fully within the first annular region, with a solution of specific Mouse IgG. Fig. 6 shows the experimental peak–peak values obtained as a function of time. The overall amplitude modulation is caused by disk wobble. There are systematic changes in the signal when the

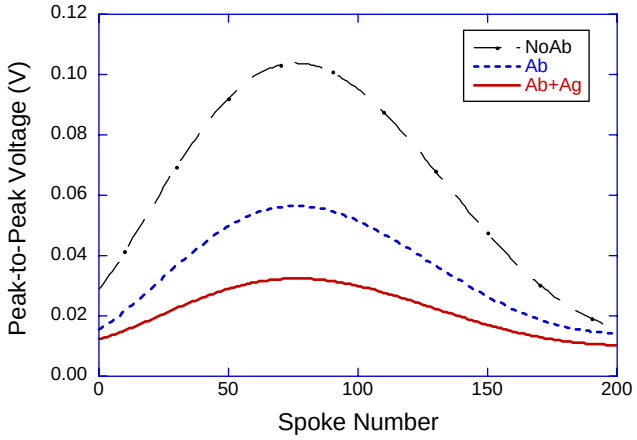

Fig. 6. Detection of the binding of antigen (mouse IgG) on a silicon BioCD. In the figure, 'Ab' refers to anti-mouse IgG and 'Ag' refers to mouse IgG. The change caused by the binding of the antigens is about 25%. This result clearly demonstrates the detection of binding.

disk is exposed to antibody and then to antigen, demonstrating the binding of the specific antigen to the immobilized antibody.

3.2. Non-specific binding

An important performance parameter for biochips is the strength of non-specific binding of the antibodies to non-target molecular species. Non-specific binding can be quantified by detecting a signal level change for antigens not specific to the antibody. We immobilized the BioCD with anti-mouse IgG and exposed part of the disk to mouse antigen, which is the specific antigen in this case, and the remaining part to BSA, which is a non-specific species. Fig. 7 shows the results of the non-specific binding experiments on silicon. The expected change in the signal from the region that was exposed to mouse IgG, the specific antigen, indicates binding. However, the region exposed to

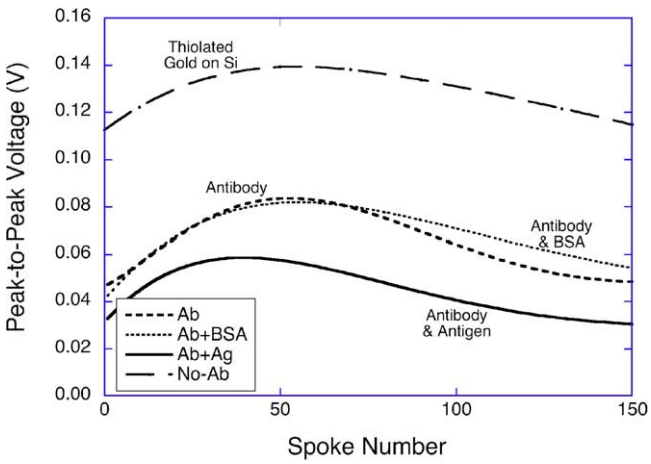

Fig. 7. Results of the non-specific binding experiments on a silicon BioCD showing small non-specific binding signal modulation.

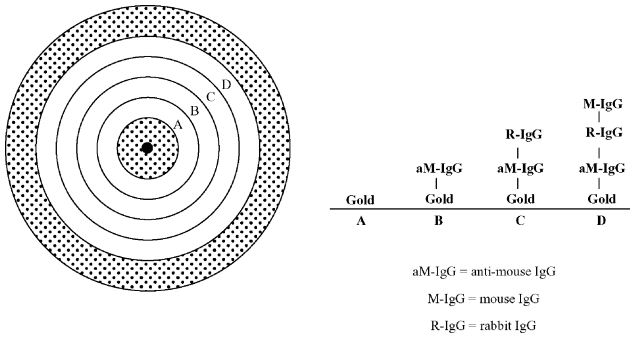

Fig. 8. Track layout for the non-specific binding and activity-blocking experiments on a dielectric mirror substrate. The specific antigen is mouse IgG. The non-specific antigen is rabbit IgG.

BSA, the non-specific antigen, shows no appreciable signal change, verifying low non-specific binding. In the figure, 'Ab' refers to anti-mouse IgG and 'Ag' refers to mouse IgG.

Experiments on a laser mirror provide a more stringent test of non-specific binding. The track sequence is shown in Fig. 8. The non-specific species in this case is rabbit IgG which is morphologically similar to the specific antigen mouse IgG and hence may be more likely to bind non-specifically. An important aspect in this experiment is the exposure to the specific antigen *after* exposure to non-specific antigen. This not only tests for non-specific binding, but also tests for blocking or inactivation of the antibody by initial exposure to the non-specific species. Such interference would prevent a multi-analyte approach. The results of the experiment are shown in Fig. 9 for only a selected number of spokes. For gold alone, the order of the peaks and dips are opposite that for silicon (compare Fig. 5) because of the high substrate reflectivity. The immobilization of the antibody lowers the valleys (at quadrature) while

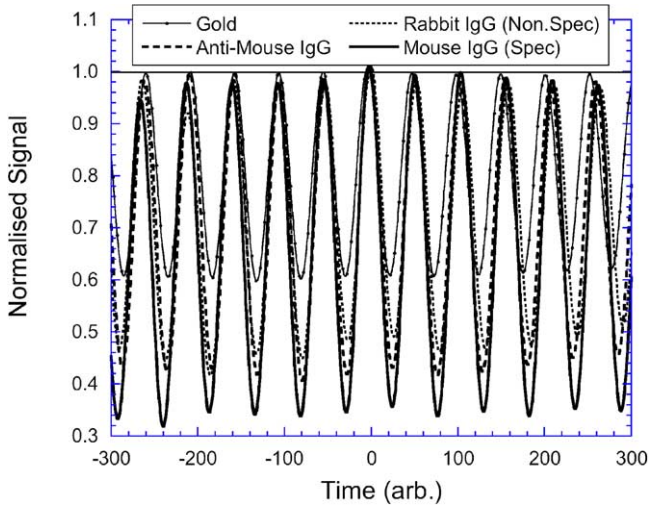

Fig. 9. Detection of Mouse IgG, and specificity of the detection scheme. The dielectric BioCD is printed with anti-mouse IgG on a dielectric mirror substrate. Incubation with non-specific rabbit IgG produces no change in the far-field diffraction intensity. Subsequent incubation with specific mouse IgG produces a further drop in the far-field diffraction intensity at quadrature.

leaving the peaks (from the land) unchanged. Exposure to the non-specific antigen, rabbit IgG, causes no additional phase change and registers no change in signal. However, subsequent exposure to the specific antigen, mouse IgG, causes an additional increment in the signal. Thus, the detection scheme is specific to the target analyte, and is not blocked by previous exposure to the non-specific antigen.

4. Conclusions and future work

The number of detected antigen molecules is estimated by considering a monolayer of immobilized antibody on a spoke (verified separately by AFM measurements) illuminated within the beam waist of the laser. This is around 10^7 molecules per spoke or about 10 femtomol per track. The sensitivity of the system described in this paper is estimated from an assumed S/N = 100 to be 10^5 molecules per spoke per track, or 100 attomol. The ultimate detection sensitivity in the shot-noise limit can be derived analytically. The signal-to-noise ratio for a phase load dϕ of Eq. (1) is

$$\frac{\mathrm{S}}{\mathrm{N}} = \frac{1}{2BW}\frac{P_0}{h\nu}\eta_\mathrm{d}\,\delta\phi^2 \tag{3}$$

where BW is the detection bandwidth, P the input laser power and η_d the quantum efficiency of the detector. For a signal-to-noise ratio equal to 2, this leads to a minimum detectable thickness

$$d_\mathrm{min} = \frac{\lambda}{2\pi(n-1)}\sqrt{\frac{BWh\nu}{\eta_\mathrm{d}P_0}} \tag{4}$$

For nominal values of BW = 1 kHz, λ = 633 nm, n = 1.35, η_d = 0.7 and P_0 = 10 mW, this leads to a minimum detectable thickness of d_min = 60 fm. For an antibody molecule with a diameter of 8 nm, this corresponds to merely 100 molecules per spoke per track, or about 0.1 attomol per track. At this level of sensitivity, it is clear that surface roughness of the disk would be the limiting noise source, preventing the shot-noise limit from being attained. However, estimates of noise contributions from surface roughness of optical flats indicate that numbers down to attomol of analyte molecules may be detectable per track using this approach. Such performance remains to be experimentally demonstrated.

In conclusion, we have successfully demonstrated the effectiveness of an interferometric approach for rapid and simultaneous multi-analyte detection. This BioCD technique has the distinct advantage of being integrated in a high-speed sensor in an optical disk format delivering high-throughput screening capabilities. One possible way to implement multi-analyte capabilities would be using micro-fluidic delivery channels for protein patterning (Papra et al., 2001). Such micro-fluidic delivery systems can take advantage of the centrifugal force provided by the spinning disk. The same channels could be used for detection in a "wet" environment. This approach would also be

useful in applications other than immunoassays including proteomics, genomics and drug screening among others.

References

Bernard, A., Renault, J.P., Michel, B., Bosshard, H.R., Delamarche, E., 2000. Microcontact printing of proteins. Adv. Mater. 12, 1067–1070.

Brecht, A., Gauglitz, G., Polster, J., 1993. Interferometric immunoassay in a Fia-system—a sensitive and rapid approach in label-free immunosensing. Biosens. Bioelectron. 8, 387–392.

Fattinger, C., Koller, H., Schlatter, D., Wehrli, P., 1993. The difference interferometer—a highly sensitive optical probe for quantification of molecular-surface concentration. Biosens. Bioelectron. 8, 99–107.

Gao, H., Sanger, M., Luginbuhl, R., Sigrist, H., 1995. Immunosensing with photo-immobilized immunoreagents on planar optical wave guides. Biosens. Bioelectron. 10, 317–328.

Hanel, C., Gauglitz, G., 2002. Comparison of reflectometric interference spectroscopy with other instruments for label-free optical detection. Anal. Bioanal. Chem. 372, 91–100.

Jenison, R., Yang, S., Haeberli, A., Polisky, B., 2001. Interference-based detection of nucleic acid targets on optically coated silicon. Nat. Biotechnol. 19, 62–65.

Kunz, R.E., 1997. Miniature integrated optical modules for chemical and biochemical sensing. Sens. Actuators B 38/39, 13–28.

La Clair, J.J., Burkart, D.M., 2003. Molecular screening on a compact disk. Org. Biomol. Chem. 1, 3244–3249.

MacBeath, G., Schreiber, S.L., 2000. Printing proteins as microarrays for high-throughput function determination. Science 289 (5485), 1760–1763.

Ostroff, R.M., Maul, D., Bogart, G.R., Yang, S., Christian, J., Hopkins, D., Clark, D., Trotter, B., Moddel, G., 1998. Fixed polarizer ellipsometry for simple and sensitive detection of thin films generated by specific molecular interactions: applications in immunoassays and DNA sequence detection. Clin. Chem. 44 (9), 2031–2035.

Pohlmann, K.C., 1992. The Compact Disc Handbook, second ed. A.-R. Editions Inc.

Papra, A., Bernard, A., Juncker, D., Larsen, N.B., Michel, B., Delamarche, E., 2001. Microfluidic networks made of poly(dimethylsiloxane), Si and Au coated with polyethylene glycol for patterning proteins onto surfaces. Langmuir 17, 4090–4095.

Silzel, J.W., Cercek, B., Dodson, C., Tsay, T., Obremski, R.J., 1998. Mass-sensing, multianalyte microarray immunoassay with imaging detection. Clin. Chem. 44 (9), 2036–2043.

Varma, M.M., Nolte, D.D., Inerowicz, D.H, Regnier, E.F., 2003. High-speed label-free multi-analyte detection through micro-interferometry. Proc. SPIE 4966 (9), 58–64.